ORIGINAL RESEARCH

Patient-Specific 3-Dimensional–Bioprinted Model for In Vitro Analysis and Treatment Planning of Pulmonary Artery Atresia in Tetralogy of Fallot and Major Aortopulmonary Collateral Arteries

Martin L. Tomov, PhD; Alexander Cetnar, BS; Katherine Do, MS; Holly Bauser-Heaton, MD, PhD;* Vahid Serpooshan, PhD*

***Background*—**Tetralogy of Fallot with major aortopulmonary collateral arteries is a heterogeneous form of pulmonary artery (PA) stenosis that requires multiple forms of intervention. We present a patient-specific in vitro platform capable of sustained flow that can be used to train proceduralists and surgical teams in current interventions, as well as in developing novel therapeutic approaches to treat various vascular anomalies. Our objective is to develop an in vitro model of PA stenosis based on patient data that can be used as an in vitro phantom to model cardiovascular disease and explore potential interventions.

***Methods and Results*—**From patient-specific scans obtained via computer tomography or 3-dimensional (3D) rotational angiography, we generated digital 3D models of the arteries. Subsequently, in vitro models of tetralogy of Fallot with major aortopulmonary collateral arteries were first 3D printed using biocompatible resins and next bioprinted using gelatin methacrylate hydrogel to simulate neonatal vasculature or second-order branches of an older patient with tetralogy of Fallot with major aortopulmonary collateral arteries. Printed models were used to study creation of extraluminal connection between an atretic PA and a major aortopulmonary collateral artery using a catheter-based interventional method. Following the recanalization, engineered PA constructs were perfused and flow was visualized using contrast agents and x-ray angiography. Further, computational fluid dynamics modeling was used to analyze flow in the recanalized model.

***Conclusions*—**New 3D-printed and computational fluid dynamics models for vascular atresia were successfully created. We demonstrated the unique capability of a printed model to develop a novel technique for establishing blood flow in atretic vessels using clinical imaging, together with 3D bioprinting–based tissue engineering techniques. Additive biomanufacturing technologies can enable fabrication of functional vascular phantoms to model PA stenosis conditions that can help develop novel clinical applications. **(*J Am Heart Assoc*. 2019;8:e014490. DOI: 10.1161/JAHA.119.014490.)**

Key Words: cardiovascular disease • cardiovascular research • catheterization • pulmonary artery stenosis • tissue engineering

Tetralogy of Fallot (TOF) with pulmonary atresia and major aortopulmonary collateral arteries (MAPCAs) is a rare congenital heart disease associated with heterogeneous and complex forms of pulmonary artery (PA) stenosis.[1–6] During development, MAPCAs often arise from the aorta or one of its branches to maintain blood supply to the lungs.[7,8] The origin, number, size, and course of these collateral arteries may vary in each patient. Current surgical strategy focuses on creating centralized PA connections through unifocalization (ie, anastomosis of the collateral arteries), followed by a right ventricular (RV) to PA conduit. This surgical procedure can be performed in a single stage or, more commonly, through palliative surgeries. Through vascular anastomosis, preservation of all lung segments is the focus for ultimate low RV pressure. While procedural success and satisfactory patient outcomes have been proven through detailed and pristine anastomosis of the pulmonary vasculature,[1] these results are not universal and are unique to one surgical team.

From the Department of Biomedical Engineering, Emory University School of Medicine and Georgia Institute of Technology, Atlanta, GA (M.L.T., A.C., V.S.); Department of Pediatrics, Emory University School of Medicine, Atlanta, GA (K.D., H.B.-H., V.S.); Children's Healthcare of Atlanta, Atlanta, GA (H.B.-H., V.S.); Sibley Heart Center at Children's Healthcare of Atlanta, Atlanta, GA (H.B.-H.).

Accompanying Figures S1 through S4 and Videos S1 through S5 are available at https://www.ahajournals.org/doi/suppl/10.1161/JAHA.119.014490

*Dr Bauser-Heaton and Dr Serpooshan contributed equally to this work.

Correspondence to: Vahid Serpooshan, PhD, 1760 Haygood Drive, NE, HSRB Building, Suite E480, Atlanta, GA 30322. Email: Vahid.serpooshan@bme.gatech.edu and Holly Bauser-Heaton, MD, PhD, 1405 Clifton Road NE, Atlanta, GA 30322. Email: bauserh@kidsheart.com

Received August 30, 2019; accepted November 7, 2019.

Clinical Perspective

What Is New?

- Additive biomanufacturing technologies such as 3-dimensional printing and bioprinting were paired with clinical imaging methods and computer fluid dynamics modeling to produce functional vascular phantoms to model cardiovascular conditions that can help develop novel clinical applications.
- Bioprinted phantoms allow for in vitro investigation of disease processes that would otherwise not be possible because of patient and animal model variability.

What Are the Clinical Implications?

- The in vitro patient-specific phantoms presented here can be used to model complex surgical interventions, such as repair of tetralogy of Fallot with major aortopulmonary collateral arteries, or other cardiovascular pathologies, such as pulmonary artery atresia, severe pulmonary vein stenosis, or total occlusive coronary lesions in a reproducible and high throughput manner.
- Our functional phantom can offer effective means to address various cardiovascular conditions, leading to improved patient outcomes in the future and more faithful in vitro disease models for novel drug and/or procedure development.

Additionally, the mechanism for stenosis along the length of these abnormal vessels is unpredictable, leading to lifelong complications secondary to distal stenosis and potential atresia of PA segments.[1,3,9,10]

Surgical and transcatheter intervention following even superb surgical PA anastomosis is not rare.[9] These distal stenoses are not only difficult to reach via surgical intervention but are notorious for persistence even after transcatheter balloon angioplasty, which is the current standard-of-care intervention. Further complicating the treatment is the requirement to maintain equal and low pressure in all lung segments, which is critical for low pulmonary vascular resistance and prevention of RV hypertension.[11] Thus, methods for potential rehabilitation, including transcatheter techniques, need to be evaluated and further developed to salvage the distal vasculature with the goal of preserving all segments of the pulmonary vascular system.[9,12] Given the complexity of distal PA stenosis in this patient population, modeling and procedural innovation is necessary to treat these stenoses effectively. Patient variation is wide and a "one approach fits all" is not possible in this population, thus highlighting the need for patient-specific modeling.

To date, additive manufacturing and, in particular, 3-dimensional (3D) printing techniques have emerged as robust engineering tools to create a variety of high-fidelity 3D models for both education and research.[13] Most common printing modalities used for these purposes include extrusion- and stereolithography-based printing systems. Extrusion 3D printers can utilize a wide range of materials, including common thermoplastic polymers, some with Food and Drug Administration approval (eg, biodegradable polylactic acid and polyvinyl alcohol polymers).[14] A main drawback to extrusion techniques is the lack of sufficient print resolution. In contrast, laser-based stereolithography 3D printers benefit from faster crosslinking processes since the entire layer is formed/cured simultaneously and at higher resolutions. Major drawbacks of stereolithography printing are the relatively limited range of photocurable resins, the extensive postprocessing steps that are usually not compatible with biological materials, and the associated costs. In addition to conventional 3D printing methods, capable of generating synthetic (nonbiological) constructs, 3D bioprinting has recently enabled fabrication of live, functional tissue and organ mimics for a variety of research and training applications in the basic sciences and medical fields.

When leveraged toward biomedical and clinical applications, 3D printing (and bioprinting) can generate accurate models of patient pathologies based on commonly used medical imaging tools such as magnetic resonance imaging, computed tomography (CT), or x-ray angiography (XA). These patient-specific 3D-printed models and phantoms of target tissues and organs have shown great potential in improving our understanding of the pathophysiology of the disease and also aid in the potential development and optimization of current surgical treatments.[15–21] In the case of TOF with MAPCAs, in particular, 3D-printed models can aid in the visualization of the precise 3D configuration of collaterals and native PAs. This is vital for studying the defect and planning corrective surgeries. However, 3D in vitro models of stenotic PAs that are capable of vascular perfusion currently do not exist. Conventional 2-dimensional and 3D vascular models have shown suboptimal capacity in representing the dynamic and complex tissue microenvironment, and animal models are less tractable with respect to genetic and environmental manipulations, complicating their translation into clinical therapies.[22,23]

Here, we begin with patient-specific CT data of a neonatal patient with TOF with MAPCAs, naive to surgical or catheter-based intervention, where we were able to create a 3D representation of the aorta and pulmonary vasculature, including the pathological MAPCA connections. These vessels were subsequently 3D printed to produce an anatomically accurate, 3D in vitro model of the vasculature, capable of perfusion under clinically relevant conditions. Additionally, an adolescent patient with TOF with dual-supply MAPCAs that were attached only through distal intraparenchymal

connections underwent imaging with 3D rotational XA in the cardiac catheterization laboratory. We then engineered an abstracted in vitro model that was used to simulate a proposed recanalization technique to treat nearly atretic vessels in which antegrade flow has been lost as a result of MAPCA stenosis and ultimate involution. Using state-of-the-art bioprinting and tissue engineering approaches, these platforms can form the basis for design and manufacturing 3D replicas of patient vasculature with specific cardiovascular conditions that could then be extrapolated into functional clinical phantoms useful in surgical procedure training and exploration of novel techniques, as well as a basis for disease modeling.[24]

Methods

Detailed methods and 3D models for the purposes of reproducing the results and procedures can be made available upon request to the corresponding author. The institutional review board at Emory University granted a waiver for this work.

Generation of Patient-Specific 3D Digital Models of Pulmonary Vasculature—3D Printing of Synthetic PA Models

Starting with a CT of vasculature from a patient with TOF and MAPCA, we extracted the 3D information that allowed us to generate the digital 3D model (stereolithography file) of the pulmonary vascular system. For this purpose, images of a neonate (aged 3 days) and an adolescent (aged 14 years) with MAPCA were used. The 3D reconstructions were hollowed using an Autodesk Meshmixer 3D modeling program to generate a shell thickness of 1 mm that could be used to perfuse the printed models. Following stereolithography creation, the right PAs of the neonate patient were 3D printed on a Form 2 stereolithography printer (Formlabs) using 2 distinct resins including the Flexible Resin and Clear (hard) Resin. Postprocessing to prepare the models involved 3 washes of 20 minutes each in pure isopropanol to remove residual noncrosslinked resin, followed by thorough drying and removal of any supports. Finally, the cleared models were UV cured for 20 minutes to stabilize their shape and physical properties, such as clarity (Clear Resin) or flexibility (Flexible Resin). Printed PA models were imaged and compared with the conventional patient's angiographic images. For our adolescent patient, images were obtained from a selective right PA angiogram with 3D rotational angiography utilizing breath hold and cardiac pacing to eliminate artifact. Using Vitrea (Toshiba) software, a stereolithography file was rendered and 3D printed on the Form 2 stereolithography printer using the Flexible Resin and Clear Resin. Printed constructs were imaged in the catheterization laboratory using XA with selective injections of contrast agent into the vascular structure to visualize the distal vascular connections to verify that our phantoms could be imaged via clinically relevant techniques.

Based on parameters gleaned from both patients, a simplified design of the in vitro phantom simulating PA atresia was generated by isolating (cropping) the 3D digital model containing a reconstructed PA and a now atretic MAPCA, from the complex anatomical model of the adolescent patient (Figure S1). Based on the generated stereolithography model, synthetic phantoms were 3D printed by the Form 2 printer, using Flexible Resin, Clear (hard) Resin, and Elastic Resin. Following printing, models were UV cured and the support structures subsequently removed. For one design of these models, an extraluminal connection (canalization) was simulated by printing a hollow channel (3.5 mm lumen) in the synthetic phantoms, followed by stenting. The connection was tested by (manually) perfusing buffer solution through the vascular structure. Based on these procedures we were able to generate an in vitro model that incorporates the critical pathological areas of distal vasculature seen in TOF with MAPCAs to be used for further in vitro studies.

GelMA Bioink Preparation

Gelatin methacrylate (gelMA) was prepared as previously described.[25,26] Briefly, porcine gelatin (Sigma) was modified with methacrylic anhydride (Sigma) at 50°C for 3 hours. The functionalized gelatin was cleared of unreacted methacrylic anhydride via reverse osmosis, lyophilized, and stored away from light at −20°C until use.[25,26] To prepare the gelMA concentration that was used to generate the PA phantom, we reconstituted 1 gram of lyophilized gelMA into 5 mL of 1X sterile PBS, to a final concentration of 20% (w/v) gelMA solution. The mixture was heated at 60°C for 30 minutes to fully dissolve the gelMA into the PBS. Subsequently, 0.5% (w/v) of Irgacure (Sigma-Aldrich) photoinitiator was added to the solution. The bioink was stored away from ambient light at 4°C until use.

Fabrication of Hybrid Biological PA Phantoms

The simplified stereolithography model simulating the PA geometry was generated as described above and used to 3D bioprint biological phantoms. The manufactured hybrid phantoms comprised 2 main parts: (1) a biological part, which was generated using gelMA hydrogel, via either casting or 3D bioprinting methods (25×14×7.5 mm); and (2) a 3D-printed synthetic housing made from the Formlabs' Flexible Resin, which housed the gelMA block. The gelMA block contained 2

parallel vessels (at 7.5 mm distance from each other) mimicking the atretic PA and an MAPCA. The vessel representing the PA was an open, thorough channel (25 mm in length), enabling perfusion through the construct, and the atretic artery, or occluded MAPCA, was simulated by a channel closed two thirds through the structure (17.5 mm in length). These vessels were both 2 mm in diameter, which is an average diameter of distal target vessels in pediatric patients with TOF and MAPCA. The 3D-printed polymeric housing allowed for inlet and outlet barbed connectors to securely connect to the device and to introduce the sheath, which then served as the entry point for the materials used for anastomosis in our proposed model (Figure S2).

The 20% gelMA solution was either cast (2.5 mL of gelMA was manually pipetted) or 3D bioprinted using a Bio X bioprinter (CELLINK) into the customized housing, followed by UV crosslinking at 80 mW/cm^2 for 10 minutes. A microscope slide and a glass coverslip were attached (glued) to cover and seal the bottom and top surfaces, respectively, which also helped to keep the models sterile. Perfusion outlets were 18G blunt needles (Nordson) with luer locks for easy and reliable connection to our perfusion tubing assembly and bioreactor, which were inserted into the 3D-printed housing. Constructs were sealed with Parafilm and stored at 4°C in the fridge until use.

In Vitro Vessel Anastomosis Procedure to Connect Atretic Vasculature

The perfusable bioprinted PA model was used to simulate a proposed interventional procedure to treat distal PA atresia. The perfusable vessel was first engaged with a sheath and imaged with Omnipaque (GE Healthcare) under fluoroscopic guidance and images were obtained utilizing biplane fluoroscopy (Toshiba). The atretic vessel was cannulated under direct fluoroscopic visualization with a coronary total occlusion wire (Pilot 1.5 g, Abbott) and a microcatheter (Turnpike, Teleflex). Subsequently, a 4F glide catheter (Terumo) was passed along the coronary wire with the microcatheter for a coaxial system to create a position for soft wire probing. A runthrough 0.14″ coronary wire (Terumo) was carefully passed into the atretic vessel lumen and the connection was subsequently established with a 3×15 mm stent (Promus Premier Everolimus-Eluting Stent, Boston Scientific Corporation). Repeat angiography was used to examine flow within vascular lumens. The procedure was performed on the benchtop (Video S1 and Figure S3) for phantom optimization and repeated in the cardiac catheterization laboratory to simulate the clinical setting (Figure S2 and Video S2). Anastomosed vessels were then manually perfused with contrast agent (Omnipaque, Novaplus) postprocedure for at least 30 seconds to verify restored flow into both vessels.

Computational Modeling of Flow in Recanalized Vascular Model

A geometrically representative CAD model of a recanalized PA model was designed (Fusion 360, Autodesk Inc), meshed, and analyzed (ANSYS Fluent, ANSYS, Inc). Inlets and outlets were 2 mm in diameter. The recanalized connection was assumed to be 3 mm in diameter at a 45° angle from the direction of flow. A mesh of >200k elements was constructed via a CellCut assembly method. Mesh solutions were considered convergent when successive mesh velocities differed by <5%. A laminar viscous solver (Navier-Stokes based) was evaluated for whole fetal blood rheological properties in a time-varying, pulsatile flow waveform. For boundary conditions, an inlet velocity and pressure outlets were prescribed. The pulsatile waveform used for the inlet is representative of clinical velocities of neonatal PA over 3 cardiac cycles (60 time steps per cycle). Constant outlet pressures (5 mm Hg) were applied at both outlets based on clinical estimates. Whole fetal blood applied constant mass density (1.06 g/cm^3)[27] with a nonlinear Carreau viscosity model (time constant: 3.313 seconds, power-law index: 0.3568, zero shear viscosity 0.056 P; infinite shear viscosity: 0.0035 P).[28] Vascular walls were assumed rigid with no-slip boundary conditions.

Results

We used CT and XA imaging data acquired during presurgical preparation to generate 3D models of patients with PA (Figure 1A and 1B, respectively). Using these images, digital models of pulmonary vasculature were constructed for both neonate (aged 3 days) (Figure 1C) and adolescent (aged 14 years) (Figure 1D) patients, with resolution that allowed for vascular network and vessel lumen reconstruction, recapitulating those of the in vivo conditions.

Multiple synthetic (resin-based) models were reliably printed for neonatal and adult patients with minimal postprocessing required, while still maintaining high-fidelity patient 3D cardiovascular structures (Figure 1E and 1F). The protocol to generate these anatomically accurate synthetic phantoms was streamlined to take 2 to 3 days to complete, starting with the clinical data, through 3D model design and optimization, and concluding with testing the manufactured vasculature mimics for retained perfusion capabilities. While somewhat long, our proposed pipeline is still within the time frame to be suitable for use as a clinical aid in future planning surgical interventions. Resins used to print synthetic PA models include high resolution (Clear Resin, Figure 1E-1 and 1F-1), highly flexible (Elastic Resin, data not shown), and a compromise between high detail and flexibility (Flexible Resin, Figure 1E-2 and 1F-2). The Clear Resin was ultimately chosen

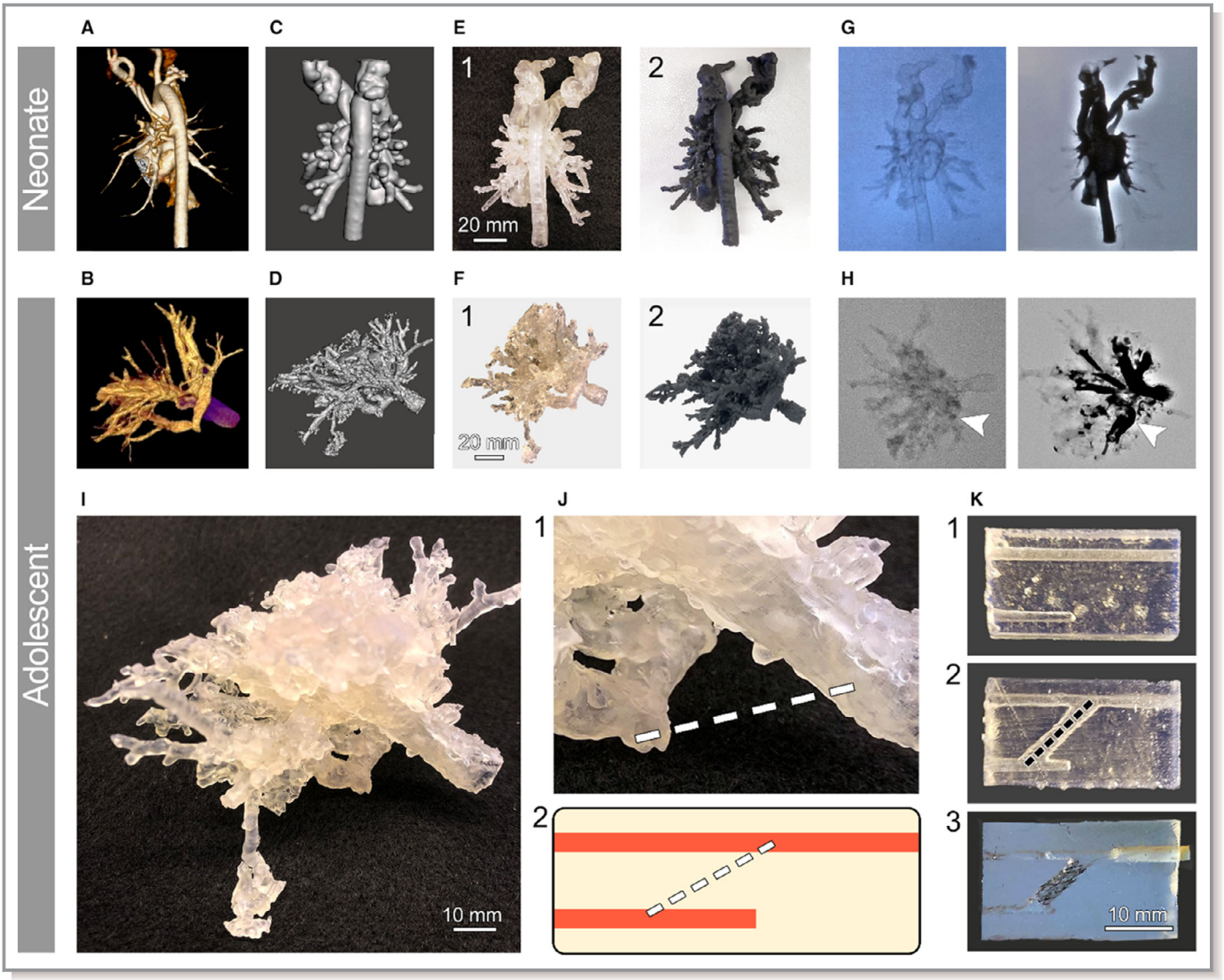

Figure 1. Patient-specific in vitro pulmonary artery atresia model. Neonatal and adult vasculature with pulmonary artery atresia pathology were imaged via computed tomography (CT) (**A**) and 3-dimensional (3D) rotational angiography (**B**). The vessel lumens were converted into 3D stereolithography files with 1-mm thickness for neonatal and adult patients (**C** and **D,** respectively). These digital models were subsequently 3D printed (**E** and **F**) using different synthetic resins, including Clear Resin (1) and Flexible Resin (2) to pinpoint the most suitable material for the phantom. Validation using x-ray angiography using iodine-based contrast agent was performed on each patient model (**G** and **H**) without (left) and after (right) contrast addition. Arrows in (**H**) mark the vascular atresia. A simplified phantom was derived from the adult patient model by isolating the 3D area that included the occluded vessel and a functional vessel (**I**). Zoomed view of this area (**J**, 1) and the extrapolated stenotic phantom (**J**, 2) are shown. Proof-of-concept synthetic models of the phantom were created to evaluate its use (**K**). Untreated model (1), anastomosed vessels model (2), and stented model (3), mimicking the proposed treatment procedure, were 3D printed using Clear Resin for phantom optimization and iteration purposes.

as the main synthetic material to print the PA models as it allowed for visualization of the vasculature and flow. The Flexible Resin was used to produce the phantom housings for the in vitro devices. The Elastic Resin, while able to create highly flexible models, did not provide distal resolution comparable to the other inks and resulted in blocked distal vessel lumens.

While CT-based stereolithography models and prints resulted in distal fusions of the PAs and veins (Figure 1C and 1E), 3D rotational XA imaging of printed TOF with MAPCA models in the cardiac catheterization laboratory generated pristine visualization of the distal vascular connections and spatial resolution of the nearly atretic vessel in an adolescent patient who underwent prior unifocalization and conduit placement (Figure 1G and 1H). We did note after generation of the stereolithography file and printing that the external smaller vasculature was not smooth in contour; however, the internal vasculature upon injection closely recapitulated the contour of the angiogram. The XA-based printed constructs closely resembled selective injections of the MAPCAs

performed on the same neonate patient 3 weeks earlier in the cardiac catheterization laboratory (Figure S4 and Video S3). The 3D reconstruction and prints highlighted each patient's right PA and the connections to the atretic beak (Figure 1H, arrows), which represented the previously ligated MAPCA. This vessel became the target for potential rehabilitation and was chosen for our in vitro device design for recanalization.

To make the phantom more applicable as a generalized in vitro tool to test proposed procedures and to improve its reproducibility, we simplified the in vitro PA device to only recapitulate the most important aspects of the proposed recanalization procedure. The simplified PA phantom consisted of an occluded (atretic MAPCA) and an open (PA) vessel with a 3-mm lumen for both (Figure 1I through 1K). The lumen diameter and the length of target vessels were kept within the range that was deemed suitable for clinical intervention. This model was utilized to simulate an extraluminal canalization procedure between the 2 vessels by printing a 3.5-mm hollow channel and subsequently stenting the connection (Figure 1K, middle and bottom). The connection was tested by (manually) perfusing buffer solution through the canalized structure (Videos S1 and S2).

Biological phantom models were 3D bioprinted or cast using 20% gelMA as bioink, while closely mimicking the lumen diameter of the native vasculature (Figure 2A and 2B). GelMA constructs were stabilized during the fabrication processes, using sacrificial pluronic, and postprinting, during the flow experiments, using a printed synthetic housing chamber (Figure 2C). The synthetic-printed bioreactor housing allowed for applying homeostatic flow rates to the construct, retained the shape and geometry of soft hydrogel, and created a reproducible perfusion setup that is reliable and scalable towards high-throughput tissue manufacturing (Figure 2C).

These hybrid phantoms of PA pathology were subsequently employed to test a model vascular anastomosis (unifocalization) procedure to recanalize the atretic artery (Figure 2D and 2E; Figure S3). To validate our phantom for recanalization success, we conceptualized a novel PA atresia treatment, where vessel anastomosis to a functional blood supply network is achieved and stabilized via a modified stent bridge (Figure 2D). While initial trials failed because of extensive damages to the vascular structure, optimized procedural technique ultimately proved successful to bridge the 2 vessels and restore robust, steady flow from the functional vessel into the target atretic vessel (Figure 2E, Figure S3; Videos S1 and S2). Using this method, we demonstrated that the proposed catheter-based recanalization approach could be used, without significant damages to the vascular structure, to reestablish flow in occluded vessels (Figure 2E). Following conducting the procedures on the benchtop (Figure S3 and Video S2), performing the technique in the cardiac catheterization laboratory under imaging guidance improved the method with regards to enhanced control and clinical relevance (Figure 2E and Video S1).

In addition to experimental work, we also present here a computational fluid dynamics (CFDs) model of the recanalized PA platform that was designed and utilized to predict blood flow patterns through the recanalized vasculature. Spatial and temporal values of velocities (vector and streamline) and wall shear stress were calculated (Figure 2F; Videos S4 and S5). The pulsatile PA cardiac waveform, ranging from 16 to 25 mm/s, used in the CFD model recapitulated the blood flow in the neonatal PA case over 3 cardiac cycles. Our model predicted peak flow velocities of 41 mm/s through the vascular structure, with maximum velocity before the anastomosis point. Flow is adequately divided at the bifurcation without significant preference for one outlet. During the deceleration phase of systole, flow recirculation is predicted at the connection's flow entrance (Figure 2F, III).

Discussion

With the recent advancements in the field of tissue engineering and biomanufacturing, specifically 3D printing and bioprinting, there is a growing interest in the development of in vitro patient-specific phantoms to model complex surgical interventions, such as TOF with MAPCA repair, or other cardiovascular pathologies, such as pulmonary vein stenosis or total occlusive coronary lesions.[29,30] Enhanced fidelity and resolution, and an expanded range of materials (inks) used in modern 3D (bio)printers have further allowed tissue engineers to develop faithful replicas of patient tissues and organs to inform patients, surgical teams, and other healthcare professionals.[13] While models like this could be done in synthetic materials, resin and thermoplastics cannot adequately support phantom cellularization, specifically in vitro cellular remodeling, as they lack the physiomechanical properties to recapitulate the native tissue microenvironment. Further, the demonstrated interventional procedure would not be possible in a synthetic model. GelMA, on the other hand, has been repeatedly shown to mimic soft tissue stiffness and support cell attachment, function, and remodeling in cellularized constructs for long periods of time. Such constructs can then also be used to model disease pathology and progression or to design and develop novel treatments and implants.[31–35] Combining such models with patient-specific stem cell–derived cardiac cells, such as cardiomyocytes and endothelial cells, can incorporate the genetic and epigenetic information of the patient into the in vitro platform and further enhance their application for various disease modeling.[36,37] In patients with TOF with MAPCAs, severe stenosis of the PA vascular tree alters flow in the other vasculature segments, which can have adverse effects on lung function and cardiovascular health as a result of elevated RV pressure of

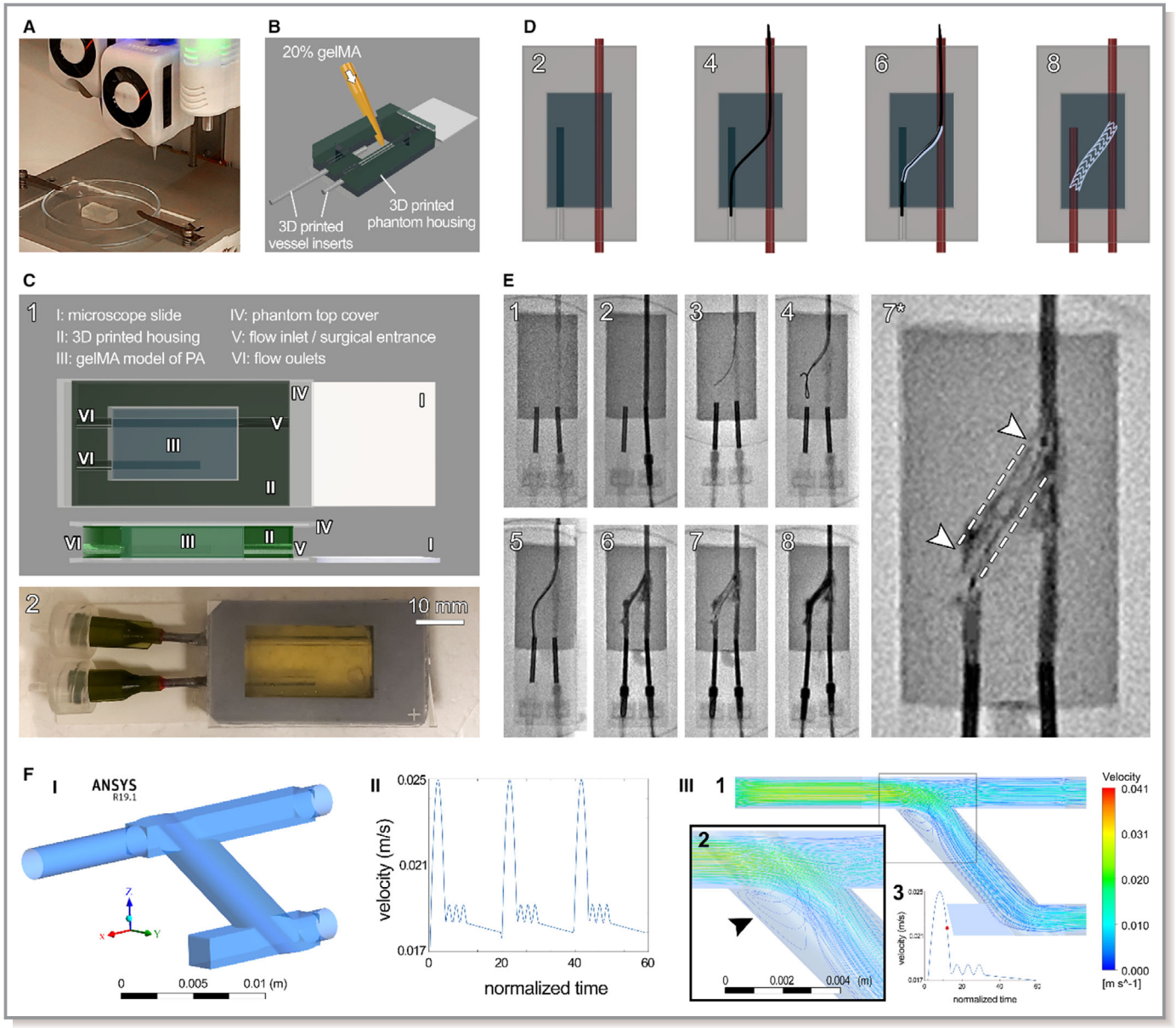

Figure 2. Bioprinted phantom for recanalization of atretic vessels. A commercial 3-dimensional (3D) bioprinter (CELLINK Bio X) was used to generate the biological model of tetralogy of Fallot with major aortopulmonary collateral arteries (MAPCAs) (**A**), which were then assembled into the 3D-printed housings. A second approach, gelatin methacrylate (gelMA) casting directly into a 3D-printed housing, was used to generate a second batch of phantoms (**B**). Render of the assembled phantom (**C**) shows its key parts (I-VI, **C**-1), with a fully assembled example shown below (**C**-2). Schematic of the proposed recanalization procedure (**D**), showing flow in only the open vessel (2), catheter bridge (4), stent introduction (6), and stent deployment with flow restored in both vessels (8). Catheterization laboratory capture of the full procedure (**E**) shows the major (1–8) steps, starting from device setup and flow test (1–2) through establishment of bridge between the vessels (3–5), stent introduction (6) and deployment (7), and finally restored flow into both vessels (8). Zoom-in of the deployed stent before flow reestablishment in both vessels is shown in (7*). The procedure was repeated 3 times. **F**, Computational fluid dynamic modeling of the stented atretic model, demonstrating (I) the computer-aided design (CAD) model, (II) normalized flow velocity waveform over the cardiac cycle prescribed, and (III, 1–3) the characteristic flow pattern during the downstroke of systole. Arrow in III-2 designates a turbulent flow region at the entry of the recanalized connection. III-3 shows one pulse of velocity waveform and the red circle highlights the time point at which the flow data were acquired. PA indicates pulmonary artery.

the patient in general.[1,11,38,39] Thus, intervention to repair or alleviate the condition must be performed as early as possible, usually no later than early childhood, in an effort to preserve the unobstructed lung segments.[39,40] The goal of such treatments is, therefore, preservation of flow in all lung segments with equal PA pressure to lead to ultimate preservation of total pulmonary vascular resistance. Thus, in our in vitro model, we focused on vessel sizes that would be prime candidates for intervention, such as recanalization or unifocalization, in a pediatric patient. Further, we wanted to

mimic the lack of flow in the affected vasculature and the complexity of blood flow restoration. This model allows future studies of flow patterns following establishment of vascular connections via our proposed procedure. The designed synthetic housing for the phantom would allow long-term perfusion of the PA constructs using bioreactor systems.

To assess the feasibility of our approach, we presented an in vitro model for vascular atresia that was successfully developed to allow anastomosis to neighboring vessels. A model technique for establishing blood flow in atretic vessels was developed using patient CT and 3D rotational data, combined with 3D printing and bioprinting methods. While CT is widely used in procedural planning in this patient population, we found it particularly challenging to have adequate resolution between major aortopulmonary collaterals and adjacent pulmonary veins. Selective injection in the vascular structure with 3D rotational angiography provided this spatial resolution and resulted in pristine visualization of the atretic MAPCA. Printing complex vascular anatomy at adequate resolution and fidelity was achieved and allowed for further development and practice of interventional procedures that can be clinically applicable in the future. As vessel anastomosis is a complicated procedure, we ensured that our model could account for the common technical challenges of the procedure, specifically relating to procedure development, equipment use (both for tracking and for intervention), and materials selection. A variety of (bio)ink materials were selected to create in vitro models with tissue environment that recapitulates what a surgical team might find when addressing MAPCA connections. Our vessel phantom was thus designed to allow imaging guidance, maintain hydrogel stiffness comparable to in vivo conditions, and allow for homeostatic flow preanastomosis and postanastomosis. We are currently working on further enhancing the in vitro model to perform additional studies in preparation for in vivo testing. While this procedure holds promise for future clinical applications, such as procedural planning for intervascular connections in the setting of vascular atresia (eg, PA, pulmonary vein, or coronary total occlusion), we acknowledge that the materials for such a procedure are limited and the risks are not negligible. Considerations for optimizing blood flow between intervascular connections must be completed and include angle of approach, diameter of connection, and maneuverability of a connection around extravascular structures such as the trachea and esophagus. An in vitro model, at this stage, holds great promise to investigate these parameters in a systematic manner with careful planning. Therefore, we propose to continue to study these parameters for intervascular connections while preparing for in vivo trials by expanding on the functional analysis of our phantoms via transcriptomics, proteomics, and in-depth cellular interactions preprocedure and postprocedure. With this work, we intend to improve PA stenosis and rescue atretic vascular segments through catheter and surgically based intervascular connection techniques. This will allow once-lost vascular segments to be incorporated into the vascular network and thereby reduce pulmonary vascular resistance in these complex patient populations who are susceptible to RV hypertension.

CFD modeling provides a robust tool to simulate blood (or culture media) perfusion within the newly established pulmonary connection in the PA model. In parallel to the experimental setup, this computational platform furthers study and optimization of geometrical, structural, biomechanical, and flow parameters in the vascular phantom (eg, diameter, location, and angle of the conduit, blood velocity, and elasticity/stiffness). Establishing a conduit for flow may temporarily provide an avenue for blood flow; however, stenosis-inducing flow patterns must be avoided or the recanalized connection may lose its patency. For example, low-velocity, directionally oscillatory flow patterns are known to correlate with arterial stenosis. Thus, evaluating a variety of connection designs and angles must be considered to avoid pathologic turbulent flows that will eventually close the newly cleared conduit.

Establishing a reproducible process to generate patient-specific 3D models that can be used in a clinical setting is an exciting development that bridges the fields of cardiovascular surgery/transcatheter intervention and tissue engineering.[41–45] A potential application of this hybrid approach would be to generate a model of the pathology to be used as a training tool in a surgical/transcatheter intervention.[46,47] Generation of an in vitro model in this particular cardiovascular condition (TOF with MAPCAs with atretic arteries), in which no specific animal models exist, allows for investigation of disease processes that would otherwise not be possible because of patient and animal variability. Combining additive manufacturing, tissue engineering, and surgical interventions with a robust CFD model can produce effective means to address various cardiovascular conditions, leading to improved patient outcomes in the future and more faithful in vitro disease models for novel drug and procedure development.

Study Limitations

Despite the great potential for improved patient outcomes, it remains a challenge to combine clinical data, additive manufacturing, tissue engineering, and disease modeling into the same ecosystem to aid in clinical outcomes or basic research. Translating patient data into printable 3D models requires specific skill sets and expertise that are not always readily available among surgical and basic science research teams. Particularly in the field of cardiovascular disease modeling, as a result of the complexities of the vascular anatomy, developing suitable stereolithography models

requires advanced cardiology and radiology rendering skills. We predict that difficulty in generating such patient-specific models will be a major limitation to incorporating 3D-printed and -bioprinted components in surgical preperation/planning and disease modeling. The resolution of clinical CT imaging techniques also leaves challenges for 3D printing as detection of vascular walls within structures, such as pulmonary veins and arteries, can be difficult. Rotational angiography, as an alternative imaging modality, for printing adds clarity as different parts of the structure are injected separately and thus resolution is improved. This technique should be interpreted with care, however, as stereolithography generation requires a shell to be created, which ends in external vascular artifact. The internal vasculature remains the same as the selective angiogram performed in the patient vascular structure.

Conclusions

In the case of bioprinted, biological phantoms, there are multiple challenges on cellularization of such bulk tissue constructs, maintaining printed cell viability and function (enabling effective diffusion/transfer of nutrients and oxygen), and long-term perfusion of constructs in vitro. It is a nontrivial approach to anastomose 2 vessels at these diameters without significant vessel/cell damage in both in vitro and in vivo settings. Preventing hemorrhage during anastomosis, mitigating potential stenosis formation, and addressing material/ink selections to fabricate a biodegradable, functional conduit must be accounted for in the future development of interventional methods using these platforms as we progress towards in vivo applications. We are aware that the presented CFD model is, of necessity, a simplified state of in vivo conditions, but we plan to expand and enhance this part of the proposed intervention planning in future works to include complex vasculature stereometry and different mechanical parameters of the walls, and also model a separate conduit that would be used to recanalize the 2 vessels.

Acknowledgments

We are grateful for the expert technical assistance and help provided by Sassan Hashemi and Timothy Slesnick.

Sources of Funding

This research was funded by National Institutes of Health grant number R00HL127295 and Emory University School of Medicine (Pediatric Research Alliance Pilot Grant and the Dean's Imagine, Innovate and Impact [I3] Research Award).

Disclosures

None.

References

1. Bauser-Heaton H, Borquez A, Han B, Ladd M, Asija R, Downey L, Koth A, Algaze CA, Wise-Faberowski L, Perry SB, Shin A, Peng LF, Hanley FL, McElhinney DB. Programmatic approach to management of tetralogy of Fallot with major aortopulmonary collateral arteries: a 15-year experience with 458 patients. *Circ Cardiovasc Interv*. 2017;10:e004952.
2. Bauser-Heaton H, Ma M, McElhinney DB, Goodyer WR, Zhang Y, Chan FP, Asija R, Shek J, Wise-Faberowski L, Hanley FL. Outcomes after aortopulmonary window for hypoplastic pulmonary arteries and dual-supply collaterals. *Ann Thorac Surg*. 2019;108:820–827.
3. Bauser-Heaton H, Ma M, Wise-Faberowski L, Asija R, Shek J, Zhang Y, Peng LF, Sidell DR, Hanley FL, McElhinney DB. Outcomes after initial unifocalization to a shunt in complex tetralogy of Fallot with MAPCAs. *Ann Thorac Surg*. 2019;107:1807–1815.
4. Carotti A, Albanese SB, Filippelli S, Rava L, Guccione P, Pongiglione G, Di Donato RM. Determinants of outcome after surgical treatment of pulmonary atresia with ventricular septal defect and major aortopulmonary collateral arteries. *J Thorac Cardiovasc Surg*. 2010;140:1092–1103.
5. Babliak OD, Mykychak YB, Motrechko OO, Yemets IM. Surgical treatment of pulmonary atresia with major aortopulmonary collateral arteries in 83 consecutive patients. *Eur J Cardiothorac Surg*. 2017;52:96–104.
6. Soquet J, Barron DJ, d'Udekem Y. A review of the management of pulmonary atresia, ventricular septal defect and major aortopulmonary collateral arteries. *Ann Thorac Surg*. 2019;108:601–612.
7. Norgaard MA, Alphonso N, Cochrane AD, Menahem S, Brizard CP, d'Udekem Y. Major aorto-pulmonary collateral arteries of patients with pulmonary atresia and ventricular septal defect are dilated bronchial arteries. *Eur J Cardiothorac Surg*. 2006;29:653–658.
8. Rabinovitch M, Herrera-deLeon V, Castaneda AR, Reid L. Growth and development of the pulmonary vascular bed in patients with tetralogy of Fallot with or without pulmonary atresia. *Circulation*. 1981;64:1234–1249.
9. Bauser-Heaton H, Borquez A, Asija R, Wise-Faberowski L, Zhang Y, Downey L, Perry SB, Koth A, Peng LF, Algaze CA, Hanley FL, McElhinney DB. Pulmonary reinterventions after complete unifocalization and repair in infants and young children with tetralogy of Fallot with major aortopulmonary collaterals. *J Thorac Cardiovasc Surg*. 2018;155:1696–1707.
10. Ligon RA, Kim DW, Vincent RN, Bauser-Heaton HD, Ooi YK, Petit CJ. Angiographic follow-up of infants and children undergoing percutaneous carotid artery interventions. *Catheter Cardiovasc Interv*. 2018;91:1301–1306.
11. Kirklin JW, Blackstone EH, Shimazaki Y, Maehara T, Pacifico AD, Kirklin JK, Bargeron LM Jr. Survival, functional status, and reoperations after repair of tetralogy of Fallot with pulmonary atresia. *J Thorac Cardiovasc Surg*. 1988;96:102–116.
12. Brown SC, Eyskens B, Mertens L, Dumoulin M, Gewillig M. Percutaneous treatment of stenosed major aortopulmonary collaterals with balloon dilatation and stenting: what can be achieved? *Heart*. 1998;79:24–28.
13. Nikitichev DI, Patel P, Avery J, Robertson LJ, Bucking TM, Aristovich KY, Maneas E, Desjardins AE, Vercauteren T. *Patient-Specific 3D Printed Models for Education, Research and Surgical Simulation*. IntechOpen. 2018.
14. Joo Y, Shin I, Ham G, Abuzar SM, Hyun S-M, Hwang SJ. The advent of a novel manufacturing technology in pharmaceutics: superiority of fused deposition modeling 3D printer. *J Pharm Investig*. 2019. Available at: https://doi.org/10.1007/s40005-019-00451-1.
15. Ehler ED, Barney BM, Higgins PD, Dusenbery KE. Patient specific 3D printed phantom for IMRT quality assurance. *Phys Med Biol*. 2014;59:5763–5773.
16. Wood RP, Khobragade P, Ying L, Snyder K, Wack D, Bednarek DR, Rudin S, Ionita CN. Initial testing of a 3D printed perfusion phantom using digital subtraction angiography. *Proc SPIE Int Soc Opt Eng*. 2015;9417:94170V.
17. Izzo RL, O'Hara RP, Iyer V, Hansen R, Meess KM, Nagesh SVS, Rudin S, Siddiqui AH, Springer M, Ionita CN. 3D printed cardiac phantom for procedural planning of a transcatheter native mitral valve replacement. *Proc SPIE Int Soc Opt Eng*. 2016;9789:978908.
18. Arconada-Alvarez SJ, Lemaster JE, Wang J, Jokerst JV. The development and characterization of a novel yet simple 3D printed tool to facilitate phantom imaging of photoacoustic contrast agents. *Photoacoustics*. 2017;5:17–24.
19. Kim MT, Park JH, Shin JH, Kim N, Kim SD, Tsauo J, Kim KY, Kim GB, Song HY. Influence of contrast agent dilution on ballon deflation time and visibility during tracheal balloon dilation: a 3D printed phantom study. *Cardiovasc Intervent Radiol*. 2017;40:285–290.

20. Meess KM, Izzo RL, Dryjski ML, Curl RE, Harris LM, Springer M, Siddiqui AH, Rudin S, Ionita CN. 3D printed abdominal aortic aneurysm phantom for image guided surgical planning with a patient specific fenestrated endovascular graft system. *Proc SPIE Int Soc Opt Eng*. 2017;10138:101380P.
21. Jahnke P, Schwarz FB, Ziegert M, Almasi T, Abdelhadi O, Nunninger M, Hamm B, Scheel M. A radiopaque 3D printed, anthropomorphic phantom for simulation of CT-guided procedures. *Eur Radiol*. 2018;28:4818–4823.
22. LaBourene JI, Coles JG, Johnson DJ, Mehra A, Keeley FW, Rabinovitch M. Alterations in elastin and collagen related to the mechanism of progressive pulmonary venous obstruction in a piglet model. A hemodynamic, ultrastructural, and biochemical study. *Circ Res*. 1990;66:438–456.
23. Kato H, Fu YY, Zhu J, Wang L, Aafaqi S, Rahkonen O, Slorach C, Traister A, Leung CH, Chiasson D, Mertens L, Benson L, Weisel RD, Hinz B, Maynes JT, Coles JG, Caldarone CA. Pulmonary vein stenosis and the pathophysiology of "upstream" pulmonary veins. *J Thorac Cardiovasc Surg*. 2014;148:245–253.
24. Anwar S, Singh GK, Miller J, Sharma M, Manning P, Billadello JJ, Eghtesady P, Woodard PK. 3D printing is a transformative technology in congenital heart disease. *JACC Basic Transl Sci*. 2018;3:294–312.
25. Shirahama H, Lee BH, Tan LP, Cho NJ. Precise tuning of facile one-pot gelatin methacryloyl (GelMA) synthesis. *Sci Rep*. 2016;6:31036.
26. Cui H, Miao S, Esworthy T, Zhou X, Lee SJ, Liu C, Yu ZX, Fisher JP, Mohiuddin M, Zhang LG. 3D bioprinting for cardiovascular regeneration and pharmacology. *Adv Drug Deliv Rev*. 2018;132:252–269.
27. Gahr M, Meves H, Schröter W. Fetal properties in red blood cells of newborn infants. *Pediatr Res*. 1979;13:1231–1236.
28. Shibeshi SS, Collins WE. The rheology of blood flow in a branched arterial system. *Appl Rheol*. 2005;15:398–405.
29. El Sabbagh A, Eleid MF, Al-Hijji M, Anavekar NS, Holmes DR, Nkomo VT, Oderich GS, Cassivi SD, Said SM, Rihal CS, Matsumoto JM, Foley TA. The various applications of 3D printing in cardiovascular diseases. *Curr Cardiol Rep*. 2018;20:47.
30. Giannopoulos AA, Mitsouras D, Yoo SJ, Liu PP, Chatzizisis YS, Rybicki FJ. Applications of 3D printing in cardiovascular diseases. *Nat Rev Cardiol*. 2016;13:701–718.
31. Honigmann P, Sharma N, Okolo B, Popp U, Msallem B, Thieringer FM. Patient-specific surgical implants made of 3D printed PEEK: material, technology, and scope of surgical application. *Biomed Res Int*. 2018;2018:4520636.
32. Vukicevic M, Mosadegh B, Min JK, Little SH. Cardiac 3D printing and its future directions. *JACC Cardiovasc Imaging*. 2017;10:171–184.
33. Serpooshan V, Hu JB, Chirikian O, Hu DA, Mahmoudi M, Wu SM. Chapter 8—4D printing of actuating cardiac tissue. In: Al'Aref SJ, Mosadegh B, Dunham S, Min JK, eds. *3D Printing Applications in Cardiovascular Medicine*. Boston: Academic Press; 2018:153–162.
34. Hu JB, Tomov ML, Buikema JW, Chen C, Mahmoudi M, Wu SM, Serpooshan V. Cardiovascular tissue bioprinting: physical and chemical processes. *Appl Phys Rev*. 2018;5:041106.
35. Serpooshan V, Mahmoudi M, Hu DA, Hu JB, Wu SM. Bioengineering cardiac constructs using 3D printing. *J 3D Print Med*. 2017;1:123–39.
36. Chang EA, Tomov ML, Suhr ST, Luo J, Olmsted ZT, Paluh JL, Cibelli J. Derivation of ethnically diverse human induced pluripotent stem cell lines. *Sci Rep*. 2015;5:15234.
37. Tomov ML, Olmsted ZT, Dogan H, Gongorurler E, Tsompana M, Otu HH, Buck M, Chang EA, Cibelli J, Paluh JL. Distinct and shared determinants of cardiomyocyte contractility in multi-lineage competent ethnically diverse human iPSCs. *Sci Rep*. 2016;6:37637.
38. Shimazaki Y, Maehara T, Blackstone EH, Kirklin JW, Bargeron LM; Jr. The structure of the pulmonary circulation in tetralogy of fallot with pulmonary atresia. A quantitative cineangiographic study. *J Thorac Cardiovasc Surg*. 1988;95:1048–1058.
39. Shimazaki Y, Tokuan Y, Lio M, Nakano S, Matsuda H, Blackstone EH, Kirklin JW, Shirakura R, Ogawa M, Kawashima Y. Pulmonary artery pressure and resistance late after repair of tetralogy of Fallot with pulmonary atresia. *J Thorac Cardiovasc Surg*. 1990;100:425–440.
40. Vaikunth SS, Bauser-Heaton H, Lui GK, Wise-Faberowski L, Chan FP, Asija R, Hanley FL, McElhinney DB. Repair of untreated older patients with tetralogy of Fallot with major aortopulmonary collaterals. *Ann Thorac Surg*. 2019;107:1218–1224.
41. Serpooshan V, Zhao M, Metzler SA, Wei K, Shah PB, Wang A, Mahmoudi M, Malkovskiy AV, Rajadas J, Butte MJ, Bernstein D, Ruiz-Lozano P. The effect of bioengineered acellular collagen patch on cardiac remodeling and ventricular function post myocardial infarction. *Biomaterials*. 2013;34:9048–9055.
42. Serpooshan V, Ruiz-Lozano P. Ultra-rapid manufacturing of engineered epicardial substitute to regenerate cardiac tissue following acute ischemic injury. *Methods Mol Biol*. 2014;1210:239–248.
43. Serpooshan V, Zhao M, Metzler SA, Wei K, Shah PB, Wang A, Mahmoudi M, Malkovskiy AV, Rajadas J, Butte MJ, Bernstein D, Ruiz-Lozano P. Use of bio-mimetic three-dimensional technology in therapeutics for heart disease. *Bioengineered*. 2014;5:193–197.
44. Wei K, Serpooshan V, Hurtado C, Diez-Cunado M, Zhao M, Maruyama S, Zhu W, Fajardo G, Noseda M, Nakamura K, Tian X, Liu Q, Wang A, Matsuura Y, Bushway P, Cai W, Savchenko A, Mahmoudi M, Schneider MD, van den Hoff MJ, Butte MJ, Yang PC, Walsh K, Zhou B, Bernstein D, Mercola M, Ruiz-Lozano P. Epicardial FSTL1 reconstitution regenerates the adult mammalian heart. *Nature*. 2015;525:479–485.
45. Mahmoudi M, Yu M, Serpooshan V, Wu JC, Langer R, Lee RT, Karp JM, Farokhzad OC. Multiscale technologies for treatment of ischemic cardiomyopathy. *Nat Nanotechnol*. 2017;12:845–855.
46. Vashistha R, Kumar P, Dangi AK, Sharma N, Chhabra D, Shukla P. Quest for cardiovascular interventions: precise modeling and 3D printing of heart valves. *J Biol Eng*. 2019;13:12.
47. Giannopoulos AA, Steigner ML, George E, Barile M, Hunsaker AR, Rybicki FJ, Mitsouras D. Cardiothoracic applications of 3-dimensional printing. *J Thorac Imaging*. 2016;31:253–272.

SUPPLEMENTAL MATERIAL

Figure S1. Schematic demonstration of the use of the novel 3D bioprinted model (right) to recapitulate the vascular atresia based on the anatomical data obtained from Tetralogy of Fallot (TOF) with major aortopulmonary collateral arteries (MAPCAs) patient (left).

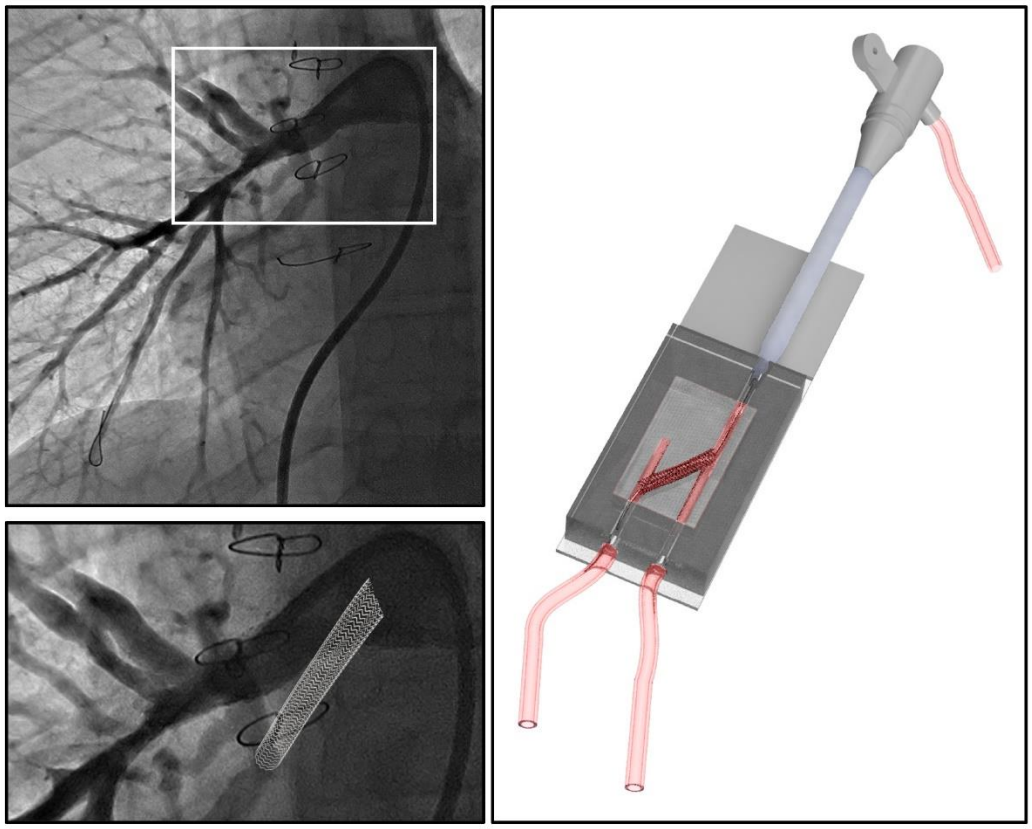

Bioengineered pulmonary artery atresia model is subsequently used to develop and optimize an anastomotic technique to establishing flow in atretic vessels.

Figure S2. Complete experimental set-up of the pulmonary artery phantom, ready for stenting.

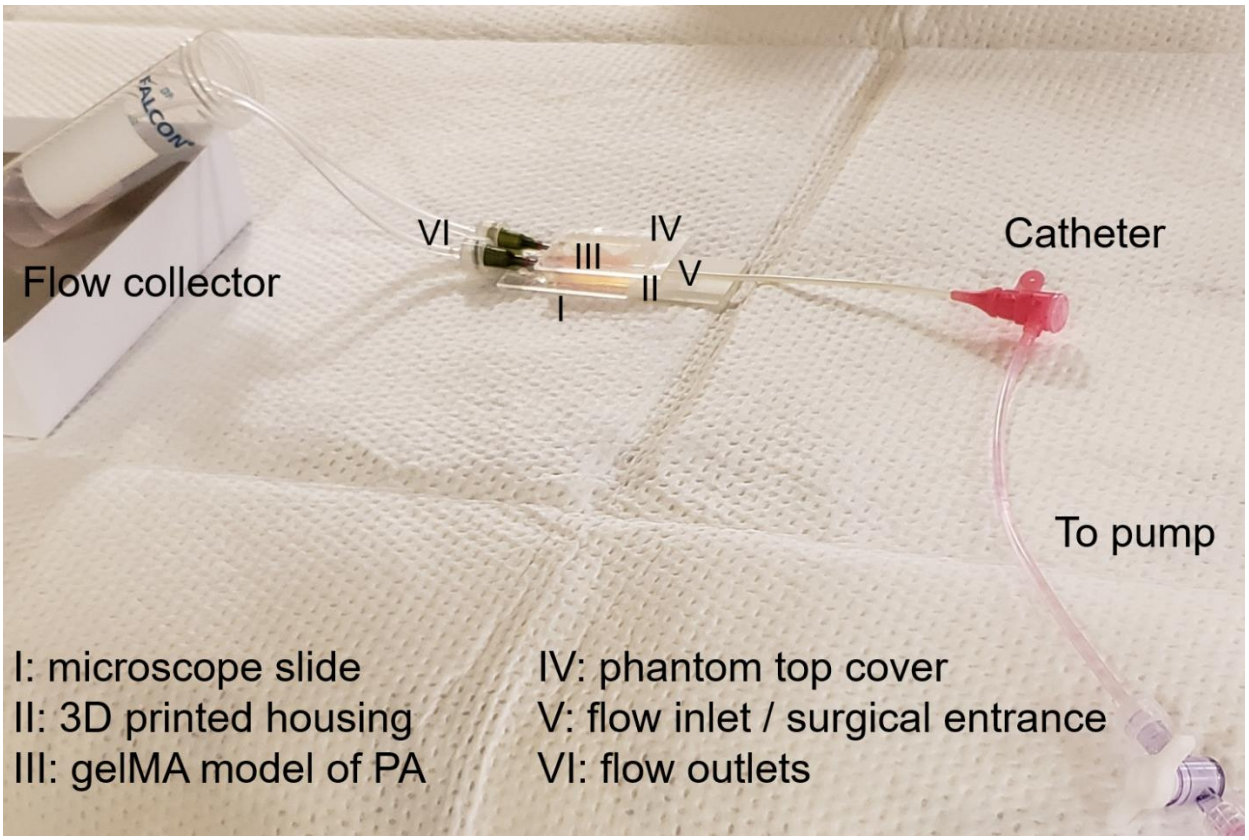

Key parts (I-VI) are highlighted, including the connection to the pump, inserted catheter and flow collector tube.

Figure S3. Process flow for the benchtop stenting procedure.

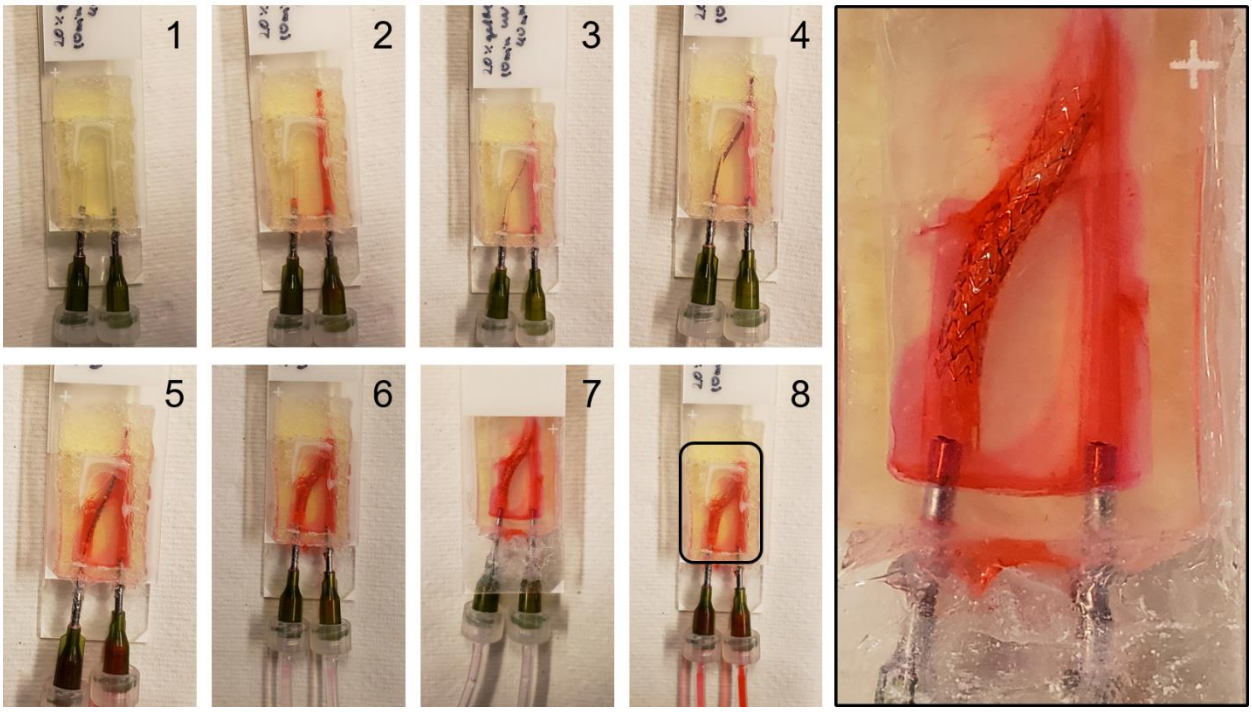

The major steps in the stenting procedure described in Figure 2E (1-8) were initially optimized in a benchtop setting prior to translating the phantom for use in an operating room.

Figure S4. Patient vasculature visualization.

Adult pulmonary artery atresia patient was injected with contrast to delineate vascular anatomy, which was then used as a benchmark quality control when developing our 3D printed phantoms.

Supplemental Movie Legends:

Movie S1. Benchtop video of PA phantom stenting procedure. Best viewed with Windows Media Player.

Movie S2. Catheterization lab video of PA phantom stenting procedure. Best viewed with Windows Media Player.

Movie S3. Contrast video of MAPCAs *in vivo*. Best viewed with Windows Media Player.

Movie S4. Velocity streamlines of recanalized model flow. Best viewed with Windows Media Player.

Movie S5. Velocity vectors of recanalized model flow. Best viewed with Windows Media Player.